



SCUOLA INTERNAZIONALE SUPERIORE DI STUDI AVANZATI

SISSA Digital Library

Improved neuron culture using scaffolds made of three-dimensional PDMS micro-lattices

This is the peer reviewed version of the following article:

Original

Improved neuron culture using scaffolds made of three-dimensional PDMS micro-lattices / Li, Sisi; Ulloa Severino, Francesco Paolo; Ban, Jelena; Wang, Li; Pinato, Giulietta; Torre, Vincent; Chen, Yong. - In: BIOMEDICAL MATERIALS. - ISSN 1748-6041. - 13:3(2018), pp. 1-11.

Availability:

This version is available at: 20.500.11767/67884 since: 2018-02-26T14:45:04Z

Publisher:

Published

DOI:10.1088/1748-605X/aaa777

Terms of use:

openAccess

Testo definito dall'ateneo relativo alle clausole di concessione d'uso

Publisher copyright

(Article begins on next page)

ACCEPTED MANUSCRIPT

Improved neuron culture using scaffolds made of three-dimensional PDMS micro-lattices

To cite this article before publication: Sisi Li *et al* 2018 *Biomed. Mater.* in press <https://doi.org/10.1088/1748-605X/aaa777>

Manuscript version: Accepted Manuscript

Accepted Manuscript is “the version of the article accepted for publication including all changes made as a result of the peer review process, and which may also include the addition to the article by IOP Publishing of a header, an article ID, a cover sheet and/or an ‘Accepted Manuscript’ watermark, but excluding any other editing, typesetting or other changes made by IOP Publishing and/or its licensors”

This Accepted Manuscript is © 2018 IOP Publishing Ltd.

During the embargo period (the 12 month period from the publication of the Version of Record of this article), the Accepted Manuscript is fully protected by copyright and cannot be reused or reposted elsewhere.

As the Version of Record of this article is going to be / has been published on a subscription basis, this Accepted Manuscript is available for reuse under a CC BY-NC-ND 3.0 licence after the 12 month embargo period.

After the embargo period, everyone is permitted to use copy and redistribute this article for non-commercial purposes only, provided that they adhere to all the terms of the licence <https://creativecommons.org/licenses/by-nc-nd/3.0>

Although reasonable endeavours have been taken to obtain all necessary permissions from third parties to include their copyrighted content within this article, their full citation and copyright line may not be present in this Accepted Manuscript version. Before using any content from this article, please refer to the Version of Record on IOPscience once published for full citation and copyright details, as permissions will likely be required. All third party content is fully copyright protected, unless specifically stated otherwise in the figure caption in the Version of Record.

View the [article online](#) for updates and enhancements.

Improved neuron culture using three-dimensional PDMS micro-lattices

Sisi Li^{ab†}, Francesco Paolo Ulloa Severino[†], Jelena Ben^c, Li Wang^{ab}, Giuletta Pinato^c,
Vincent Torre^c and Yong Chen^{ab*}

^a*PASTEUR, D épartement de chimie, École normale sup érieure,
UPMC Univ. Paris 06, CNRS, PSL Research University, 75005 Paris, France*

^b*Sorbonne Universit és, UPMC Univ. Paris 06,
École normale sup érieure, CNRS, PASTEUR, 75005 Paris, France*

^c*Neurobiology Sector, International School for Advanced Studies (SISSA),
via Bonomea, 265, 34136 Trieste, Italy*

[†]*These authors contributed equally to this work*

Abstract: Tissue engineering strives to create functional components of organs with different cell types *in vitro*. One of the challenges is to fabricate scaffolds for three-dimensional (3D) cell culture under physiological conditions. Of particular interesting is to investigate the morphology and function of the central nervous system (CNS) cultured using such scaffolds. Here, we used an elastomer, polydimethylsiloxane (PDMS), to produce lattice-type scaffolds from a photolithography defined template. The photomask with antidot arrays was spin-coated by a thick layer of resist and downward mounted on a rotating stage at angle of 45°. After exposure for three or more times keeping the same exposure plan but rotated by the same angle, the photoresist was developed to produce a 3D porous template. Afterward, a pre-polymer mixture of PDMS was poured in and cured, followed by a resist etch, resulting in lattice-type PDMS features. Before cell culture, the PDMS lattices were surface functionalized. Culture test has been done using NIH-3T3 cells and primary hippocampal cells from rats, showing homogenously cell infiltration and 3D attachment. As expected, a much higher cell number was found in 3D PDMS lattices than in 2D culture. We also found a higher neuron to astrocyte ratio and a higher degree of cell ramification in 3D culture compared to 2D culture, due to the change of scaffold topography and the elastic properties of the PDMS micro-lattices. Our results demonstrate that the 3D PDMS micro-lattices improve the survival and growth of cells as well as the network formation of neurons. We believe that such an enabling technology is useful for research and clinical applications including disease modeling, regenerative

* Corresponding author. Ecole Normale Sup érieure, 24 rue Lhomond, 75231 Paris, France. Tel.: +33 1 44322421; Fax: +33 1 44322402. E-mail address: yong.chen@ens.fr (Y. Chen).

1
2
3 32 medicine, and drug discovery/drug cytotoxicity studies.
4
5
6 33 **Keywords:** Biofabrication, Scaffold, PDMS lattice, Cell culture
7
8 34
9
10
11
12
13
14
15
16
17
18
19
20
21
22
23
24
25
26
27
28
29
30
31
32
33
34
35
36
37
38
39
40
41
42
43
44
45
46
47
48
49
50
51
52
53
54
55
56
57
58
59
60

Accepted Manuscript

1. Introduction

Cell adhesion, migration, proliferation and differentiation are guided by topographic and biochemical cues, which can now be engineered *in vitro* by sophisticated technologies [1]. The previous studies, however, were mostly devoted to the two-dimensional (2D) patterns using photolithography, soft-lithography, nanoimprint lithography and similar techniques [2-4]. Alternatively, non-lithographic techniques such as electrospinning, solvent casting, particulate leaching, etc. have been used to produce stochastic scaffolds [5-7]. More recently, 3D plotting [8-11], fused deposition molding [12, 13], stereo-lithography [14-16], self-propagating photopolymer waveguide processing [17-20], etc., are emerged as rapid prototyping techniques. These techniques are promising but generally of low resolution [21], time-consuming [22], or not biocompatibility for advanced cell assays [23].

In this work, we fabricated well-defined and elastomeric three-dimensional (3D) micro-lattices as scaffolds for neuron culture and neural network formation. Polydimethylsiloxane (PDMS), a widely used elastomer for casting and microfluidic device making, has been chosen because of its non-toxic and easy-processing properties [24-26]. In addition, the Young's module of PDMS is relatively low (0.4 - 4 MPa) and it can be regulated by changing the ratio between catalytic and basic components [27, 28]. Furthermore, the effective Young's module of the substrates made of PDMS micropillars or micro-tripods can be adjusted to match the tissue stiffness (e.g. <1KPa for brain slices) [29]. Besides, PDMS shows high optical transparency throughout the ultraviolet and visible wavelengths [30], which makes it an ideal material for 3D observation of cell behaviors in 3D scaffold in *in vitro*. The fabrication of 3D PDMS scaffolds by layer-by-layer construction has already been reported, showing the relevance of the scaffolds for culture studies [31]. Finally, it has been demonstrated that the micropatterned structures made of PDMS, pre-seeded with neurons, can be used to repair primary motor (M1) cortex lesion which induced a strong motor deficit [32]. Here, we fabricated lattice-type 3D PDMS structures using conventional photolithography and soft-lithography techniques. The conventional photolithography is used to produce 3D templates in a thick layer of resist by backside exposure with an UV light at defined incident angles. Soft lithography is used to cast PDMS into the resist templates, resulting in lattice-type PDMS features after the resist etching. The lattice parameters, i.e. thickness, indication angle and node-to-node space of the lattice units, are adjustable to produce symmetrical and asymmetrical 3D features. The PDMS replica with different geometry parameters are then used to culture NIH-3T3 cell line and primary hippocampal neuron cells of rats. The aim of this work is to fabricate a 3D cell culture platform for

1
2
3 67 applications in basic research and biomedical engineering. By using conventional lithography
4 68 techniques, 3D PDMS micro-lattices of different geometry could be produced and our results showed
5 69 improved survival and formation of neuron networks under optimal culture conditions, thus allowing
6 70 us to envisage *in vitro* 3D brain models and to overcome the barriers to the central nervous system
7 71 regeneration. The possibility to peel off the 3D structure of PDMS will further open a route for the
8 72 applications of the device for *in vivo* studies.
9

14 73 2. Experimental methods

17 74 **Chemicals and materials:** AZ40XT photoresist and AZ developer 726MIF developer were
18 75 purchased from MicroChemicals GmbH. Chrome photoplates coated with AZ1518 photoresist
19 76 @ 5300 Å thickness were from Nanofilm Inc, USA. PDMS (RTV615 Kit) was from Momentive.
20 77 Fibronectin (FN) was from Biopur AG. Dulbecco's minimum essential medium (DMEM),
21 78 L-glutamine, penicillin/streptomycin (P/S), 0.05% Trypsin-EDTA, Dulbecco's modified
22 79 phosphate-buffered saline (DPBS), PBS tablets, minimum essential medium (MEM), fetal
23 80 bovine serum (FBS), gentamycin, goat anti mouse immunoglobulin (Ig) G1 Alexa Fluor® 488,
24 81 goat anti-mouse IgG2a Alexa Fluor® 594, Fluo4-AM and Pluronic F-127 20% solution in
25 82 DMSO were purchased from Life Technologies. Rhodamine B, fungizone, paraformaldehyde
26 83 (PFA), Triton-X-100 (TX), bovine serum albumin (BSA), sodium azide,
27 84 4,6-diamidino-2-phenylindole (DAPI), Hoechst 33342, fluorescein isothiocyanate
28 85 (FITC)-labelled Phalloidin, poly-L-ornithin, D-glucose, Hepes, apo-transferrin, insulin,
29 86 D-biotin, vitamin B12, cytosine-β-D-arabinofuranoside (Ara-C), glial fibrillary acidic protein
30 87 (GFAP) and Dimethyl sulfoxide (DMSO) anhydrous, were all purchased from Sigma-Aldrich,
31 88 Matrigel was purchased from Corning, anti-β-tubulin III (TUBJ1) antibodies were purchased
32 89 from Covance.
33
34
35
36
37
38
39
40
41
42
43
44

46 90 **Fabrication of 3D templates:** The photolithography process was described in **Fig. 1a**. A
47 91 homemade rotating stage was fixed under collimated UV light with a 45 ° angle of inclination
48 92 (**Fig. 1b**). A dot array was created on the positive photoresist on the chrome photoplate using a
49 93 micro pattern generator (μPG 101, Heidelberg, Germany). After UV exposure, the plate was
50 94 developed in photoresist developer. The photoresist of exposed dot area was dissolved and then
51 95 the exposed chrome dot array was etched in chrome etchant. The rest photoresist was removed
52 96 with acetone. Then, the chrome mask with antidot array is ready to use in the following 3D
53 97 lattice mould fabrication. AZ40XT photoresist was spin-coated on the chrome mask at a speed
54
55
56
57
58
59
60

1
2
3 98 of 1800 rpm for 20 s to reach a thickness of approximately 40 μm . After baking on a hot plate at
4
5 99 126 $^{\circ}\text{C}$ for 7 min, it was mounted on the rotation stage with the photoresist downward for
6
7 100 backside UV exposure. Each exposure was performed for 90 s with a UV beam at 365 nm (9.2
8
9 101 mW/cm^2). The stage was rotated after each exposure along the major axis of the mask surface to
10 102 have an equal incident angle. After soft baking at 105 $^{\circ}\text{C}$ for 2 min, the resist was developed in
11
12 103 AZ726MIF developer for 2 min and rinsed with deionized (DI) water, resulting in a 3D porous
13
14 104 template as shown in the inserted SEM image of **Fig. 1c**.

15
16 105 **Pattern transfer:** A pre-polymer of PDMS mixture at 1:5 ratio was poured on the porous
17
18 106 template and degassed in vacuum to remove the bubbles. After solidification at 80 $^{\circ}\text{C}$ for 2 h,
19
20 107 the AZ resist was dissolved in acetone with ultrasonic (80 mW, 20 min). PDMS layer was then
21 108 separated from the Cr mask, resulting in a 3D truss structures adhered to the bottom substrate
22
23 109 (**Fig.1d**).

24
25 110 **SEM imaging:** The fabricated AZ templates, the PDMS replica and the PDMS replica with cells
26
27 111 were sputter-coated (Quorum technologies Sputter K675XD) with 5 nm gold and observed under a
28
29 112 scanning electron microscope (Hitachi S-800) operated at 10 kV,

30
31 113 **NIH-3T3 cell culture:** The 3D PDMS lattice was sterilized with autoclave at 120 $^{\circ}\text{C}$ for 30 min.
32
33 114 After drying in an oven at 120 $^{\circ}\text{C}$ for 2 h, it was treated with plasma (Plasma Cleaner, Harrick) for 3
34
35 115 min and incubated in 50 $\mu\text{g}/\text{ml}$ fibronectin in DPBS at room temperature for 30 min. NIH-3T3 cells
36 116 were prepared in a culture flask in 37 $^{\circ}\text{C}$ incubator with 5% CO_2 . The culture medium is DMEM
37
38 117 consisting 10% FBS, 1% L-glutamine, 0.1% P/S and 0.01% fungizone. After dissociation in a 0.05%
39
40 118 Trypsin-EDTA solution and centrifugation, cells were seeded on the surface of PDMS lattice at a
41
42 119 density of 1×10^4 cells/ cm^2 .

43
44 120 **Hippocampal neuron culture:** Hippocampal neurons from Wistar rats (P2-P3) were prepared in
45
46 121 accordance with the guidelines of the Italian Animal Welfare Act, and their use was approved by the
47 122 Local Veterinary Service, the SISSA Ethics Committee board and the National Ministry of Health
48
49 123 (Permit Number: 630-III/14) in accordance with the European Union guidelines for animal care
50
51 124 (d.1.116/92; 86/609/C.E.). The animals were anaesthetized with CO_2 and sacrificed by decapitation,
52
53 125 and all efforts were made to minimize suffering. The dissection procedure for the hippocampus
54 126 isolation were done as suggested elsewhere [33] and then modified as described below.

55
56
57 127 All substrates (2D glass coverslips, 2D PDMS and 3D PDMS) were treated with air plasma-cleaner
58 128 in order to facilitate cell adhesion and at the end sterilized with an UV lamp. Soon after the
59
60

1
2
3 129 substrates were coated with 50 µg/ml poly-L-ornithin overnight and coated with Matrigel just before
4
5 130 cells seeding. Dissociated cells from isolated hippocampus were plated at a concentration of 6×10^5
6
7 131 cells/ml on each substrate in Neural Medium (MEM with GlutaMAX™ supplemented with 10%
8
9 132 FBS, 0.6% D-glucose, 15 mM Hepes, 0.1 mg/ml apo-transferrin, 30 µg/ml insulin, 0.1 µg/ml
10
11 133 D-biotin, 1 µM vitamin B12, and 2.5 µg/ml gentamycin). After 48 hours, 2 µM Ara-C was added to
12
13 134 the culture medium to block glial cell proliferation, and the concentration of FBS was decreased to
14
15 135 5%. Half of the medium was changed every 2–3 days. The neuronal cultures were maintained in an
16
17 136 incubator at 37 °C, 5% CO₂ and 95% relative humidity.

18 137 **Confocal imaging of PDMS lattice and NIH-3T3 cells:** Before cell loading, the PDMS lattice was
19
20 138 treated with plasma for 3 min and immersed in 100 mM Rhodamine B in DI water for overnight.
21
22 139 NIH-3T3 cells were fixed in 4% PFA for 30 min and then permeabilized in PBS containing 0.5% TX
23
24 140 for 30 min. After blocked in blocking buffer (0.1% TX, 3% BSA, 0.1% sodium azide in PBS) for 30
25
26 141 min again, cell skeleton and nuclei were stained with 5 µg/mL phalloidin-FITC and 300 nM DAPI in
27
28 142 PBS for 30min, respectively. All the procedures were operated at room temperature and there were
29
30 143 PBS rinsing three times between each solution change. The samples were imaged under the Carl
31
32 144 Zeiss laser scanning microscopes LSM 710.

33 145 **Morphological and immunocytochemical analysis.** Cells were fixed in 4% paraformaldehyde
34
35 146 containing 0.15% picric acid in PBS, saturated with 0.1 M glycine, permeabilized with 0.1% Triton
36
37 147 X-100, saturated with 0.5% BSA in PBS and then incubated for 1 h with primary antibodies: mouse
38
39 148 monoclonal GFAP, anti-β-tubulin III (TUJ1) antibodies. The secondary antibodies were goat anti
40
41 149 mouse immunoglobulin (Ig) G1 Alexa Fluor® 488, goat anti-mouse IgG2a Alexa Fluor® 594, and
42
43 150 the incubation time was 30 min. Nuclei were stained with 2 µg/ml in PBS Hoechst 33342 for 5 min.
44
45 151 All the incubations were performed at room temperature (20–22 °C). The cells were examined using
46
47 152 a Leica DM6000 fluorescent microscope equipped with DIC and fluorescence optics, CCD camera
48
49 153 and Volocity 5.4 3D imaging software (PerkinElmer, Coventry, UK). The fluorescence images were
50
51 154 collected with a 40X magnification and 0.5 NA objective. Image J by W. Rasband (developed at the
52
53 155 U.S. National Institutes of Health and available at <http://rsbweb.nih.gov/ij/>) was used for image
54
55 156 processing.

56
57 157 **Calcium Imaging.** The cells were incubated with 4 µM of the cell-permeable calcium dye
58
59 158 Fluo4-AM, dissolved in DMSO anhydrous, and Pluronic F-127 20% solution in DMSO at a ratio of
60
159 1:1 in Neural Medium at 37 °C for 1 hour. After incubation, the cultures were washed for 30 min

1
2
3 160 with Ringer's solution (145 mM NaCl, 3 mM KCl, 1.5 mM CaCl₂, 1 mM MgCl₂, 10 mM glucose
4
5 161 and 10 mM Hepes, pH 7.4) and then transferred to the stage of a Nikon Eclipse Ti-U inverted
6
7 162 microscope, an HBO 103 W/2 mercury short arc lamp (Osram, Munich, Germany), a mirror unit
8
9 163 (exciter filter BP 465–495 nm, dichroic 505 nm, emission filter BP 515–555) and an Electron
10 164 Multiplier CCD Camera C9100-13 (Hamamatsu Photonics, Japan). The experiments were performed
11
12 165 at RT, and images were acquired using the NIS Element software (Nikon, Japan) with an S-Fluor
13
14 166 20x/0.75 NA objective at a sampling rate of 5 Hz with a spatial resolution of 256 × 256 pixels for 10–
15
16 167 20 min. To avoid saturation of the signals, excitation light intensity was attenuated by ND4 and ND8
17 168 neutral density filters (Nikon).
18
19

20 169 **Statistical Analysis.** Data are shown as the mean ± s.e.m from at least three neuronal cultures. For
21
22 170 the morphological analysis of immunofluorescence images, n refers to the number of images
23
24 171 analysed. The number of replicates and statistical tests used for each experiment are mentioned in the
25
26 172 respective figure legends or in the Results and discussion section. Significance was set to *p < 0.05,
27 173 **p < 0.01 and ***p < 0.001.
28
29

30 174 **3. Results and discussion**

31 32 33 175 **3.1 Fabrication of PDMS micro-lattices**

34
35
36 176 Contact lithography is commonly used in research laboratories to replicate the 2D patterns by
37
38 177 UV exposing a photoresist layer spin coated on a substrate through a photomask in direct contact
39
40 178 with the resist. To reach the highest resolution and the best pattern stability, we spun coat a thick
41
42 179 resist layer directly on the photomask and then performed the sequential steps with the same
43
44 180 substrate until the release of the PDMS replica (**Fig. 1a**). Since all steps are bench process and the
45
46 181 photomask can be used for many times, this fabrication technique remains straightforward and low
47
48 182 cost.

49 183 The SEM image of the PDMS replica in **Fig.1d** shows a 3D lattice feature with tetrahedral-type
50
51 184 unit-cell originated from the same aperture, defined by the antidote array on the 2D photomask and
52
53 185 the three directional UV exposures. Since the symmetry, the porosity and the interconnectivity may
54
55 186 all affect the cell culture performance, we fabricated 3D lattices of PDMS with different geometry
56
57 187 parameters.

58 188 We firstly studied the pattern geometry by rotating 120° or 90° the sample stage after each
59
60

1
2
3 189 exposure, resulting in a tripod structure (**Fig. 2a**) or a four-fold symmetry (**Fig. 2b**). Asymmetric
4 unit-cell can also be achieved by changing the rotation angle after each exposure. **Fig. 2c- 3e** show
5 190 asymmetrical lattice structures by rotating the sample stage three times with angle of 60° - 60° - 240° ;
6
7 191 90° - 90° - 180° , and 150° - 150° - 60° respectively. We also evaluated the fabrication performance by
8
9 192 changing the resist thickness and the incident angle of the UV light. **Fig. 3a1** and **a2** show the SEM
10 193 images of the PDMS lattices obtained with initial resist layer thickness of $40\ \mu\text{m}$ and $25\ \mu\text{m}$,
11
12 194 respectively. **Fig. 3b1** and **b2** show the SEM images of the PDMS lattices obtained with an UV
13
14 195 incident angle is 60° and 45° respectively. As can be seen, the resulted beam angle of the structure is
15 196 around 35° and 28° , respectively, which are in agreement with the calculation based on Snell' law.
16
17 197
18

19
20 198 The geometry of the PDMS lattices is primarily determined by the antidot diameter and pitch
21 199 size of the photomask. By varying the diameter and pitch size of the antidot but keeping the same
22 lattice height ($40\ \mu\text{m}$), we produced 3D PDMS lattices of different geometry. As shown by the SEM
23 200 images of **Fig. 4a** and **4b** (pitch size $40\ \mu\text{m}$, diameter $20\ \mu\text{m}$ and $15\ \mu\text{m}$) and **Fig. 4c** and **4d** (pitch
24
25 201 size $80\ \mu\text{m}$, diameter $20\ \mu\text{m}$ and $15\ \mu\text{m}$), the bigger the diameter, the smaller the node-to-node space.
26 202 If the pore size is too large, the resulted features look more like 3D pillars (**Fig. 4e**). **Figure 5** shows
27 the PDMS features obtained with triangle arrays of antidots with $4\ \mu\text{m}$ diameter and three different
28 203 pitch sizes: $15\ \mu\text{m}$ (**Fig. 5a1** and **a2**), $18\ \mu\text{m}$ (**Fig. 5b1** and **b2**) and $24\ \mu\text{m}$ (**Fig. 5c1** and **c2**),
29
30 204 respectively. For larger pitch sizes, the lattice feature collapses due to insufficient mechanical
31
32 205 strength, as showed in **Fig. 5d**. By changing gradually the lattice spacing in the same mask, we could
33 206 achieve a 3D gradient lattice as showed in **Fig. 5e**. Finally, the fabricated PDMS structures could be
34
35 207 peeled off (**Fig. S1**), making it possible to be used for other purposes such as microfluidic
36
37 208 integration.
38
39 209
40 210
41

42 211 **3.2 Biocompatibility test with NIH-3T3 cell line**

43
44
45 212 We choose $40\ \mu\text{m}$ -height and three-fold symmetric PDMS lattices with $6\ \mu\text{m}$ diameter and $28\ \mu\text{m}$
46 213 pitch size (**Fig. 6a**) for cell culture test. Before sterilization, we stained the PDMS lattice with
47 214 Rhodamine (red) for easy structure observation under laser confocal microscopy. Then, we seeded
48
49 215 NIH-3T3 cells on the lattice surface and cultured them for 2 days. Thanks to the optical transparency
50
51 216 of PDMS, we clearly observed adhesion and extension of actin filaments along the 3D lattice surface
52
53 217 under confocal microscopy (**Fig. 6b** and **6c**). Here, actin filaments and nuclei were respectively
54
55 218 stained by FITC (green) and DAPI (blue). From **Fig. 6h-j**, we also observed the actin filaments
56
57 219 crossed the free space of the 3D lattice features, which should be more tissue-like for *in vitro* studies.
58
59
60

1
2
3 220 The 3D embedment of cell nuclei (**Fig. 6d**) and cell cytoskeleton (**Fig. 6e and 6f**) in the 3D
4
5 221 micro-lattice of PDMS both provide the evidence of natural cuboidal cell geometry, not like often
6
7 222 observed flatten feature in conventional 2D cultures. However, the shape of the nuclei could be
8
9 223 deformed by reducing the pitch size of the lattice and this deformation is inversely proportional to
10 224 the spacing between the lattice features (**Fig. 6g**). Previously, it has been shown that both stem cell
11
12 225 proliferation and differentiation were correlated to the cell shape [34, 35]. The PDMS lattices with
13
14 226 defined geometry could be potentially applied in stem cell research.

16 227 **3.3 Culture of primary hippocampal neurons**

17
18
19 228 Primary hippocampal neurons are commonly used to study 3D network formation on substrates
20
21 229 made by different materials [7, 36]. Here, we used hippocampal neurons from rats to co-culture
22
23 230 neurons and astrocytes and show the possibility of a 3D neuronal network formation with the help of
24 231 a PDMS lattice of 15 μm diameter, 80 μm pitch size and ~ 40 μm heights (**Fig. 6**). Cells were
25
26 232 homogeneously distributed on the structure (**Fig. 7a**) and were able to form an interconnected and
27
28 233 mature network after 8 days *in vitro* (DIV) (**Fig. 7b**). From the SEM images both glia cells (**Fig. 6c**)
29
30 234 and neurons (**Fig. 7d**) showed a three-dimensional morphology characterized by rounder cell body
31 235 and neurites projected in all the directions. Glia cells show a flat but ramified morphology whereas
32
33 236 neurons have thinner processes (**Fig. 7e**) that, once contacted the surface either of other cells or of
34
35 237 the PDMS, highly ramify. These details show a good interaction between cells and material that is
36
37 238 extremely important in tissue engineering. Moreover, slight bending of the pillars can be observed
38 239 (**Fig. 7a and 7b**) due to the cell interaction with the PDMS features. In turn, the cell adhesion forces
39
40 240 might be determined [37, 38].

41
42 241 Immunostaining for neuronal and astrocytes markers, TUJ-1 and GFAP respectively (**Fig. 8**),
43
44 242 confirmed the observation made from the SEM images. Compared to the standard glass (**SI Fig. S2**)
45
46 243 and to the flat 2D PDMS substrates (**Fig. 8a**), on the 3D PDMS substrates (**Fig. 8b**), we can observe
47 244 a complex morphological ramification of both neurons and astrocytes. Besides, we found a higher
48
49 245 cell population density (215 cell/ mm^2 , 220 cell/ mm^2 and 544 cell/ mm^2 respectively) on the 3D
50
51 246 PDMS lattice, due to the three-dimensionality of the substrates which offer more surfaces for cell
52
53 247 adhesion. The increase of the cell density in 3D lattices can also be attributed to improved cellular
54 248 microenvironment, in consistent with the previous finding for rat primary hippocampal and cortical
55
56 249 cultures in PDMS micro channels [39, 40]. On 3D PDMS 51% cells are neurons and 31% are
57
58 250 astrocytes, the remained part is not identified cells (e.g. microglia), while only 33.3 % and 40.3 % of
59
60

1
2
3 251 cells are neurons on the Glass and 2D-PDMS respectively.
4

5
6 252 Clearly, the neuron density in 3D environment is significant higher than that 2D culture but the
7 difference in astrocyte density is less remarkable between 3D and 2D cultures (Glass: 33.3% of
8 253 neurons, 59.3% of astrocytes; 2D PDMS: 40.3% of neurons, 58.1% of astrocytes) (**Fig 8c**). The
9 254 calcium activity recordings of growing neurons on 3D PDMS lattice (**Fig. 8d**) show that they are
10 healthy and alive and that the proposed method is reliable for further studies and applications. In
11 255 particular, this method offers a new platform to reconstruct 3D *in vitro* neuronal network with
12 ramified and *in vivo*-like morphology, thanks to more appropriate topographical cues and elastic
13 256 properties of the substrate, compared to the bare glass and the flat 2D PDMS. Therefore, we can
14 257 assess that the 3D-PDMS lattices improve the survival and growth of the neurons and support the
15 neural network formation and maturation. Consequently, improved drug screening and
16 258 electrophysiological experiments can be expected. Finally, due to the fact that the PDMS lattices can
17 be peeled off from the substrate (**Supp. Fig.2**), it would be interesting to use them in tissue
18 259 engineering and transplantation assays [32].
19 260
20 261
21 262
22 263
23 264
24
25 264
26
27
28

29 265 **4. Conclusion**

30
31

32 266 Here we report a fabrication process of PDMS micro-lattices using backside photolithography at
33 different incident angles and soft lithography for 3D casting. The fabricated 3D lattices were used to
34 267 evaluate cell culture performance using NIH-3T3 cell line and primary hippocampal neurons of rats.
35 Homogenous cell infiltration and 3D attachment were observed using different optical techniques.
36 268 Increased cell number and neuron percentage as well as improved cell ramification were found
37 comparing to the 2D culture showing the great potential of the proposed culture system. Since the
38 269 geometry and the interconnectivity of the PDMS lattice could be precisely tuned, more systematic
39 270 studies can be developed. The proposed fabrication process is straightforward and simple, which can
40 probably be applied to a number of *in vitro* and *in vivo* studies.
41 271
42
43 272
44 273
45
46 274
47
48
49 275

50 276 **Acknowledgments**

51

52 277 This work was supported by European Commission through project contract (Neuroscaffolds)
53 and Agence de Recherche Nationale under contract No. ANR-13-NANO-0011-01 (Pillarcell). We
54 278 want to thank also Mattia Fanetti for his assistance during the SEM imaging sessions.
55 279
56
57 280
58
59
60

References

1. Théry, C., et al., *Isolation and characterization of exosomes from cell culture supernatants and biological fluids*. Current protocols in cell biology, 2006: p. 3.22. 1-3.22. 29.
2. Kidambi, S., et al., *Cell adhesion on polyelectrolyte multilayer coated polydimethylsiloxane surfaces with varying topographies*. Tissue engineering, 2007. **13**(8): p. 2105-2117.
3. Karuri, N.W., et al., *Biological length scale topography enhances cell-substratum adhesion of human corneal epithelial cells*. Journal of cell science, 2004. **117**(15): p. 3153-3164.
4. Li, S., et al., *Fabrication of gelatin nanopatterns for cell culture studies*. Microelectronic Engineering, 2013. **110**: p. 70-74.
5. Shen, F., et al., *A study on the fabrication of porous chitosan/gelatin network scaffold for tissue engineering*. Polymer international, 2000. **49**(12): p. 1596-1599.
6. Sherwood, J.K., et al., *A three-dimensional osteochondral composite scaffold for articular cartilage repair*. Biomaterials, 2002. **23**(24): p. 4739-4751.
7. Tang, Y., et al., *Patch method for culture of primary hippocampal neurons*. Microelectronic Engineering, 2017. **175**: p. 61-66.
8. Landers, R. and R. Mülhaupt, *Desktop manufacturing of complex objects, prototypes and biomedical scaffolds by means of computer - assisted design combined with computer - guided 3D plotting of polymers and reactive oligomers*. Macromolecular Materials and Engineering, 2000. **282**(1): p. 17-21.
9. Landers, R., et al., *Fabrication of soft tissue engineering scaffolds by means of rapid prototyping techniques*. Journal of materials science, 2002. **37**(15): p. 3107-3116.
10. Ang, T., et al., *Fabrication of 3D chitosan-hydroxyapatite scaffolds using a robotic dispensing system*. Materials Science and Engineering: C, 2002. **20**(1): p. 35-42.
11. Landers, R., et al., *Rapid prototyping of scaffolds derived from thermoreversible hydrogels and tailored for applications in tissue engineering*. Biomaterials, 2002. **23**(23): p. 4437-4447.
12. Zein, I., et al., *Fused deposition modeling of novel scaffold architectures for tissue engineering applications*. Biomaterials, 2002. **23**(4): p. 1169-1185.
13. Hutmacher, D.W., et al., *Mechanical properties and cell cultural response of polycaprolactone scaffolds designed and fabricated via fused deposition modeling*. Journal of biomedical materials research, 2001. **55**(2): p. 203-216.
14. Bertsch, A., H. Lorenz, and P. Renaud, *3D microfabrication by combining microstereolithography and thick resist UV lithography*. Sensors and Actuators A: Physical, 1999. **73**(1): p. 14-23.
15. Melchels, F.P., et al., *Mathematically defined tissue engineering scaffold architectures prepared by stereolithography*. Biomaterials, 2010. **31**(27): p. 6909-6916.
16. Lee, K.-W., et al., *Poly (propylene fumarate) bone tissue engineering scaffold fabrication using stereolithography: effects of resin formulations and laser parameters*. Biomacromolecules, 2007. **8**(4): p. 1077-1084.
17. Schaedler, T.A., et al., *Ultralight metallic microlattices*. Science, 2011. **334**(6058): p. 962-965.
18. Kisailus, D., A.J. Jacobsen, and C. Zhou, *Three-dimensional biological scaffold and method*

- 1
2
3 324 of making the same. 2013, Google Patents.
4
5 325 19. Jacobsen, A.J., *Optically oriented three-dimensional polymer microstructures*. 2008, Google
6 326 Patents.
7 327 20. Kisailus, D., A.J. Jacobsen, and C. Zhou, *Three-dimensional biological scaffold*
8 328 *compromising polymer waveguides*. 2012, Google Patents.
10 329 21. Zhang, B., et al., *3D printing of high-resolution PLA-based structures by hybrid*
11 330 *electrohydrodynamic and fused deposition modeling techniques*. Journal of Micromechanics
12 and Microengineering, 2016. **26**(2): p. 025015.
13 331
14 332 22. Bassoli, E., et al., *3D printing technique applied to rapid casting*. Rapid Prototyping Journal,
15 333 2007. **13**(3): p. 148-155.
16 334 23. Renbutsu, E., et al., *Preparation and biocompatibility of novel UV-curable chitosan*
17 335 *derivatives*. Biomacromolecules, 2005. **6**(5): p. 2385-2388.
19 336 24. Kane, R.S., et al., *Patterning proteins and cells using soft lithography*. Biomaterials, 1999.
20 337 **20**(23): p. 2363-2376.
21 338 25. Singhvi, R., et al., *Engineering cell shape and function*. Science, 1994. **264**(5159): p.
22 339 696-698.
24 340 26. Takayama, S., et al., *Patterning cells and their environments using multiple laminar fluid*
25 341 *flows in capillary networks*. Proceedings of the National Academy of Sciences, 1999. **96**(10):
26 342 p. 5545-5548.
28 343 27. Wang, Z., A.A. Volinsky, and N.D. Gallant, *Crosslinking effect on polydimethylsiloxane*
29 344 *elastic modulus measured by custom - built compression instrument*. Journal of Applied
30 345 Polymer Science, 2014. **131**(22).
32 346 28. Johnston, I., et al., *Mechanical characterization of bulk Sylgard 184 for microfluidics and*
33 347 *microengineering*. Journal of Micromechanics and Microengineering, 2014. **24**(3): p. 035017.
34 348 29. Migliorini, E., et al., *Acceleration of neuronal precursors differentiation induced by substrate*
35 349 *nanotopography*. Biotechnology and bioengineering, 2011. **108**(11): p. 2736-2746.
37 350 30. Yoon, Y., D.-W. Lee, and J.-B. Lee, *Fabrication of optically transparent PDMS artificial*
38 351 *lotus leaf film using underexposed and underbaked photoresist mold*. Journal of
39 352 Microelectromechanical Systems, 2013. **22**(5): p. 1073-1080.
41 353 31. Mata, A., et al., *A three-dimensional scaffold with precise micro-architecture and surface*
42 354 *micro-textures*. Biomaterials, 2009. **30**(27): p. 4610-4617.
43 355 32. Vaysse, L., et al., *Micropatterned bioimplant with guided neuronal cells to promote tissue*
44 356 *reconstruction and improve functional recovery after primary motor cortex insult*.
45 357 Biomaterials, 2015. **58**: p. 46-53.
47 358 33. Beaudoin III, G.M., et al., *Culturing pyramidal neurons from the early postnatal mouse*
48 359 *hippocampus and cortex*. Nature protocols, 2012. **7**(9): p. 1741-1754.
50 360 34. Kumar, G., et al., *The determination of stem cell fate by 3D scaffold structures through the*
51 361 *control of cell shape*. Biomaterials, 2011. **32**(35): p. 9188-9196.
52 362 35. Kumar, G., et al., *Freeform fabricated scaffolds with roughened struts that enhance both stem*
53 363 *cell proliferation and differentiation by controlling cell shape*. Biomaterials, 2012. **33**(16): p.
54 364 4022-4030.
55 364 36. Severino, F.P.U., et al., *The role of dimensionality in neuronal network dynamics*. Scientific
56 365 Reports, 2016. **6**.
57 366
58 366
59
60

1
2
3
4
5
6
7
8
9
10
11
12
13
14
15
16
17
18
19
20
21
22
23
24
25
26
27
28
29
30
31
32
33
34
35
36
37
38
39
40
41
42
43
44
45
46
47
48
49
50
51
52
53
54
55
56
57
58
59
60

37. Li, J., et al., *Culture substrates made of elastomeric micro-tripod arrays for long-term expansion of human pluripotent stem cells*. *Journal of Materials Chemistry B*, 2017. **5**(2): p. 236-244.
38. Fu, J., et al., *Mechanical regulation of cell function with geometrically modulated elastomeric substrates*. *Nature methods*, 2010. **7**(9): p. 733-736.
39. Habibey, R., et al., *A microchannel device tailored to laser axotomy and long-term microelectrode array electrophysiology of functional regeneration*. *Lab on a Chip*, 2015. **15**(24): p. 4578-4590.
40. Habibey, R., et al., *A multielectrode array microchannel platform reveals both transient and slow changes in axonal conduction velocity*. *Scientific reports*, 2017. **7**: p. 8558.

1
2
3 **Figure caption**

4 379
5 380
6 381 **Figure 1** Fabrication of the PDMS 3D lattice. (a) The fabrication process flow; (b) Backside UV
7 exposure at incident angles; (c) SEM top view of the fabricated AZ40XT 3D template and; (d) SEM
8 side view of the replicated PDMS 3D lattices. The diameter of antidots on Cr mask is 4 μm diameter
9 and the period is 18 μm . Scale bar is 10 μm .
10
11 384

12
13 385
14 **Figure 2** SEM images of symmetrical and asymmetrical PDMS 3D lattices. (a) 3-fold symmetry; (b)
15 4-fold symmetry; Asymmetry with three side vertex angles: (c) 60° - 60° - 240° ; (d) 90° - 90° - 180° ; (e)
16 150 $^\circ$ -150 $^\circ$ -60 $^\circ$. Scale bar is 10 μm .
17
18 388

19
20 389
21 **Figure 3** SEM images of PDMS 3D lattices obtained with initial resist layer thickness of 40 μm (a1)
22 and 25 μm (a2) and member incident angles of 35 $^\circ$ (b1) and 28 $^\circ$ (b2), respectively. Scale bar is 10
23 391
24 μm .
25 392

26
27 393
28 **Figure 4** SEM images of PDMS 3D lattices with different diameter resulted from different pore size.
29 (a) 20 μm diameter, 40 μm pitch size; (b) 15 μm diameter, 40 μm pitch size; (c) 20 μm diameter, 80
30 395
31 μm pitch size; (d) 15 μm diameter, 80 μm pitch size (e) 30 μm diameter, 80 μm pitch size. Scale bar:
32 396
33 100 μm
34
35

36 398
37 **Figure 5** SEM images of PDMS 3D lattices with 4 μm diameter but different pitch sizes: (a) 15 μm ;
38 399 (b) 18 μm ; (c) 24 μm ; (d) 28 μm . (e) pitch size changing from 12.5 μm to 18.5 μm . (a1), (b1), (c1),
39 400 (d) and (e) are top view images. (a2), (b2) and (c2) are side view images. Scale bar is 10 μm .
40
41 401
42

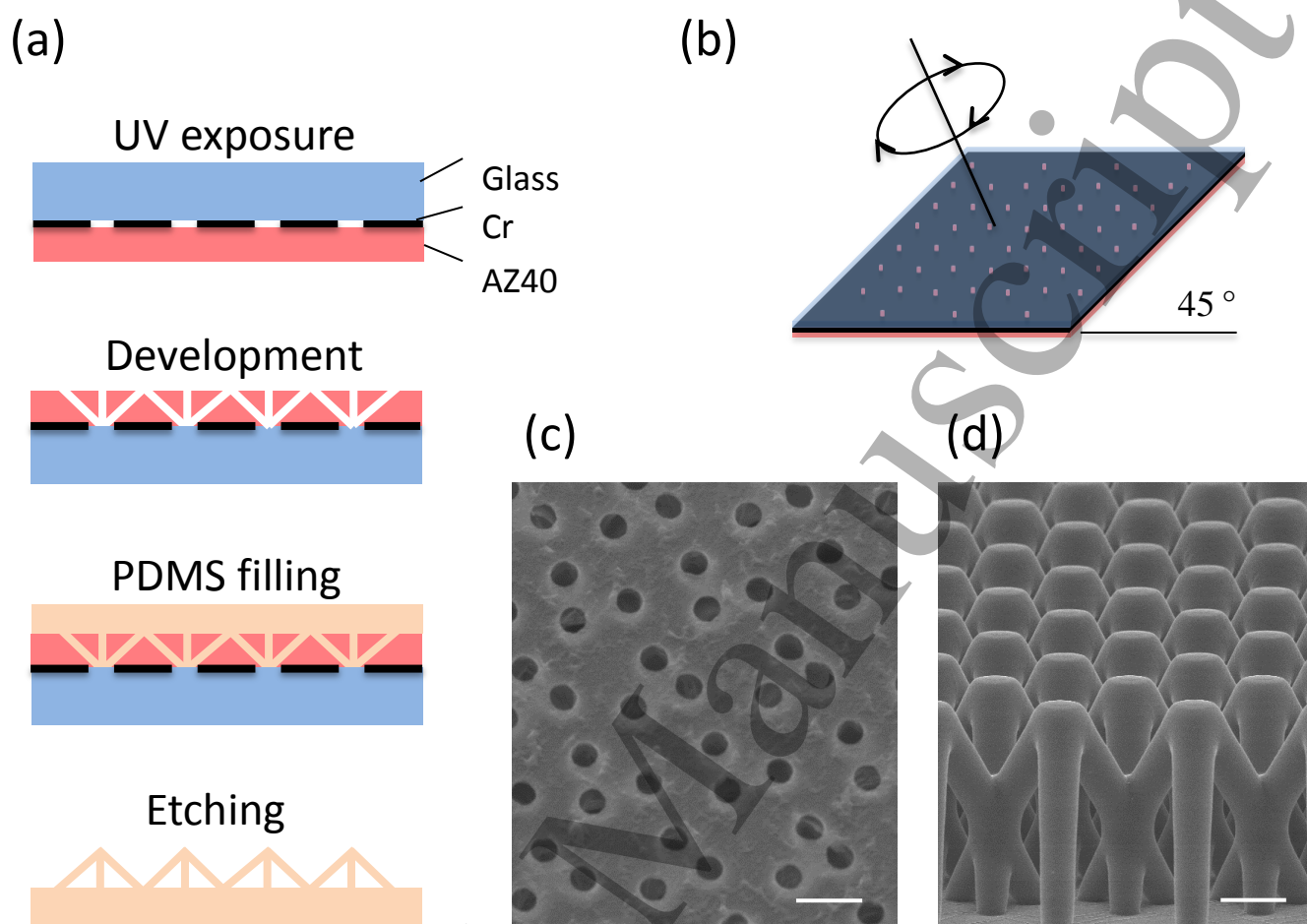
43 402
44 **Figure 6** NIH-3T3 cells in PDMS 3D lattices after culture for 2 days. (a) 3D view of a confocal
45 403 Z-stack of PDMS lattice of 6 μm diameter, 28 μm pitch size and 40 μm height. (b) 3D view of a
46 404 confocal Z-stack of cell actin filaments adhered on the lattice surface. (c) Merged image of (a) and
47 405 (b). (d) 3D view of a confocal Z-stack of cell nuclei trapped in the PDMS lattice of (a). (e) Enlarged
48 406 image of (d) but rotated in 3D space to clearly show the cell nuclei 3D distribution in the PDMS
49 407 lattice. (f) Nuclei shape of the cells in (e). (g) Z-slice of cells in the PDMS lattice of 4 μm diameter,
50 408 14 μm pitch size and 40 μm height. (h) Z-slice of cells in the PDMS lattice of (a). (i)(j) SEM images
51 409 of actin filaments crossing the free space of the PDMS lattice.
52
53 410
54
55 411
56
57
58
59
60

1
2
3
4
5
6
7
8
9
10
11
12
13
14
15
16
17
18
19
20
21
22
23
24
25
26
27
28
29
30
31
32
33
34
35
36
37
38
39
40
41
42
43
44
45
46
47
48
49
50
51
52
53
54
55
56
57
58
59
60

Figure 7 Primary hippocampal neuron culture in PDMS 3D lattices: (a-b) SEM images hippocampal co-culture after 8 DIV. (c-f) Enlarged view of the SEM images showing glia cell (g) and neuron (n) as well as the dendritic arborization and neural attachment on the PDMS surface (e,f).

Figure 8 Morphological differences among 2D (a) and 3D (b) PDMS substrates. One way ANOVA assuming normal distribution was performed to determine whether there was a significant differences between the glass (n=4), 2D-PDMS (n=3), 3D-PDMS (n=4) with respect to the number of neurons and astrocytes (c) for mm² after 8 DIV. (2D-PDMS vs 3D-PDMS $p < 0,001$; Glass vs 3D-PDMS $p < 0,001$). Example traces of calcium activity from neurons growth on 3D PDMS lattice (d).

Figure 1



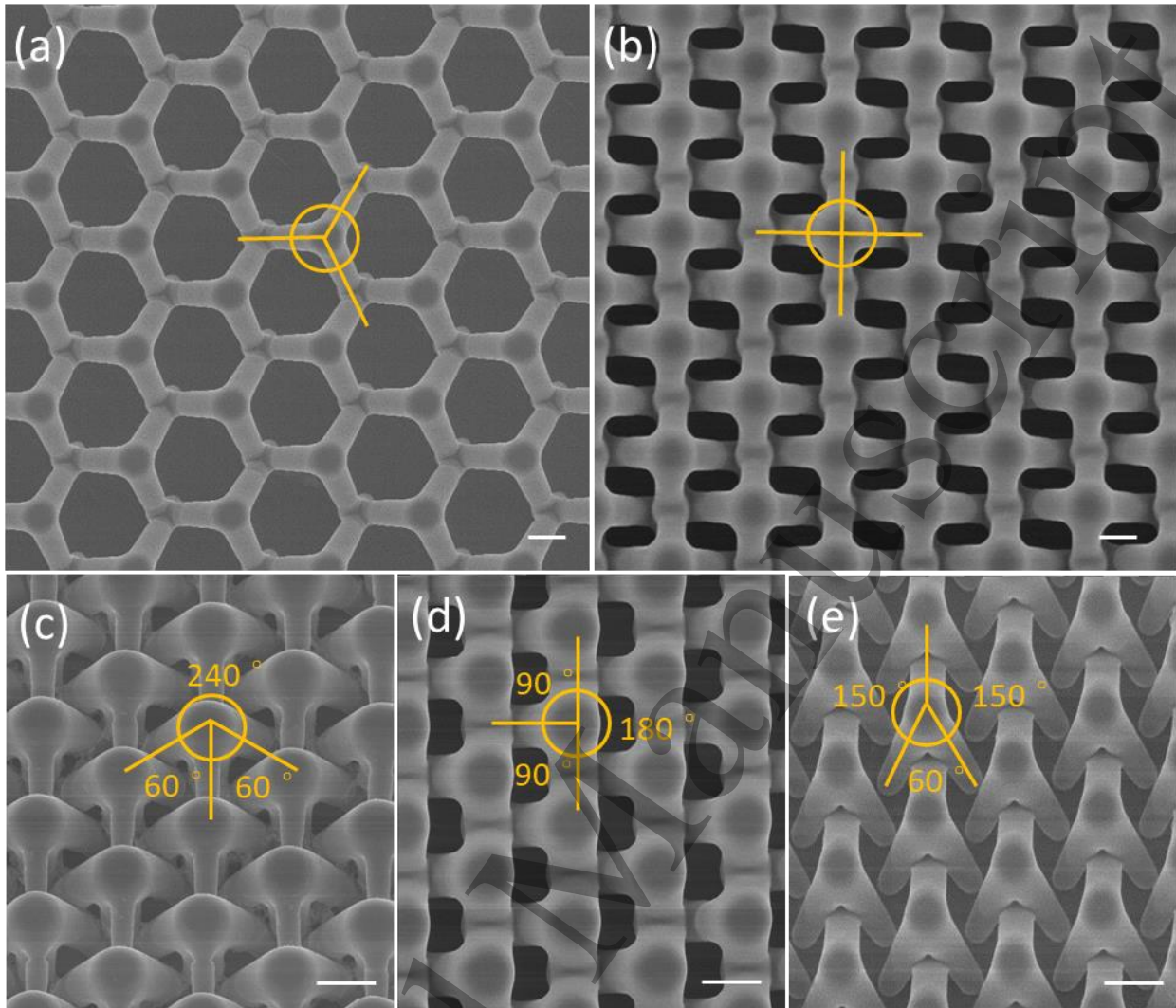
1
2
3
4
5
6
7
8
9
10
11
12
13
14
15
16
17
18
19
20
21
22
23
24
25
26
27
28
29
30
31
32
33
34
35
36
37
38
39
40
41
42
43
44
45
46
47
48
49
50
51
52
53
54
55
56
57
58
59
60426 Figure 2
427

Figure 3

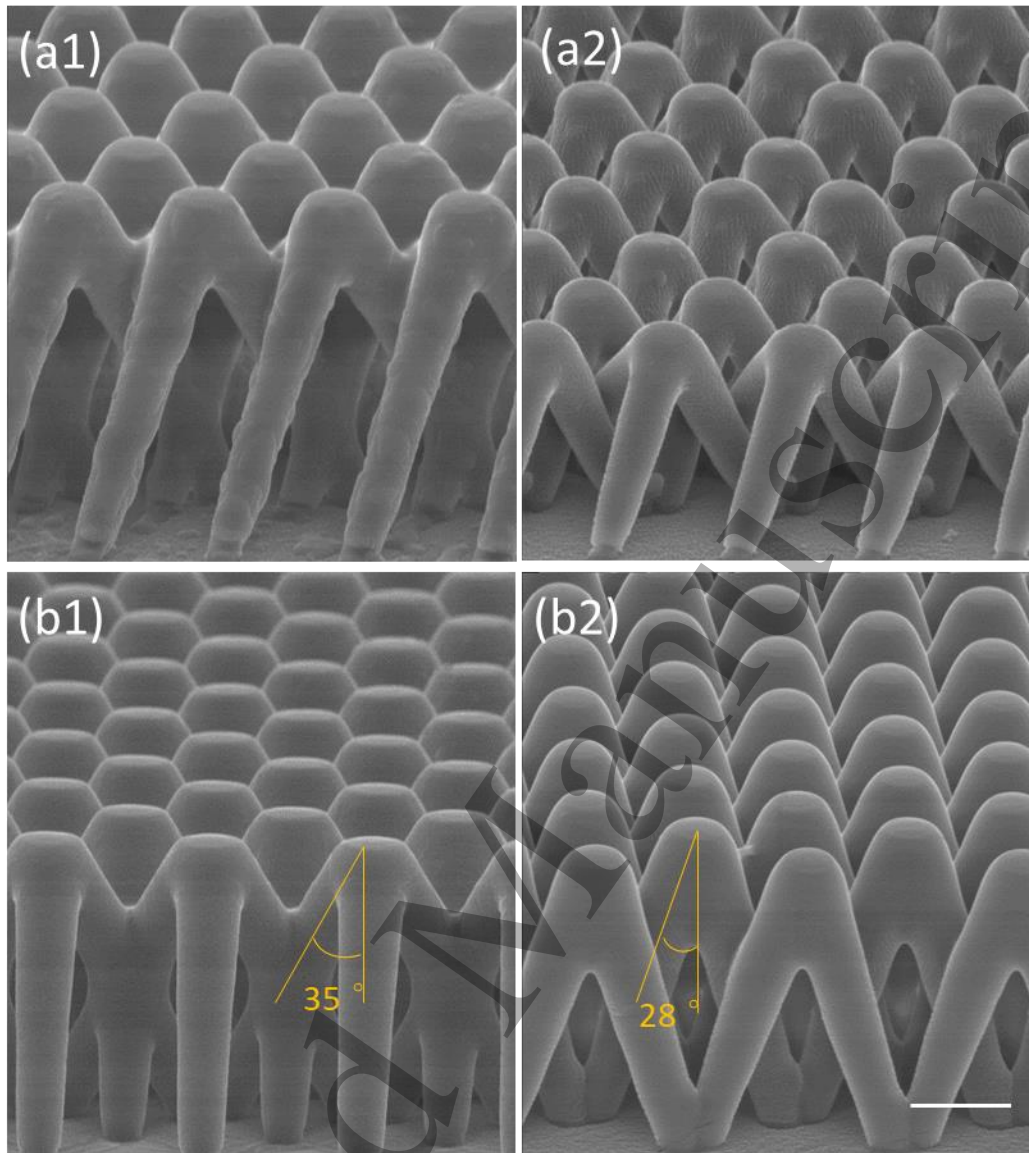
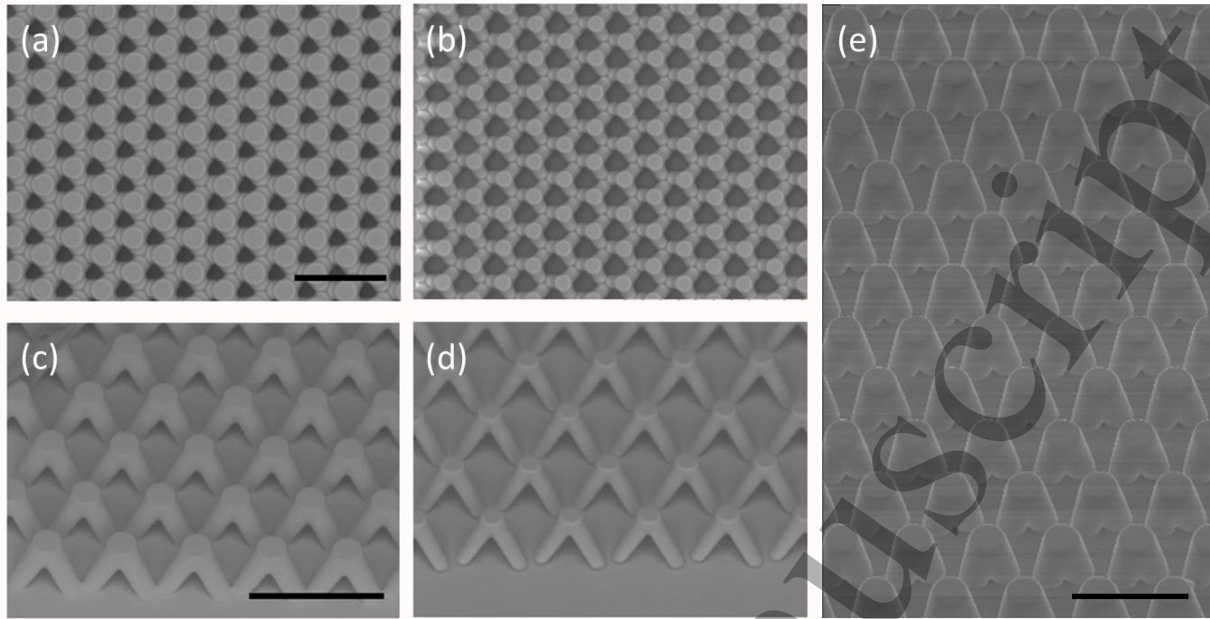


Figure 4



440 Figure 5

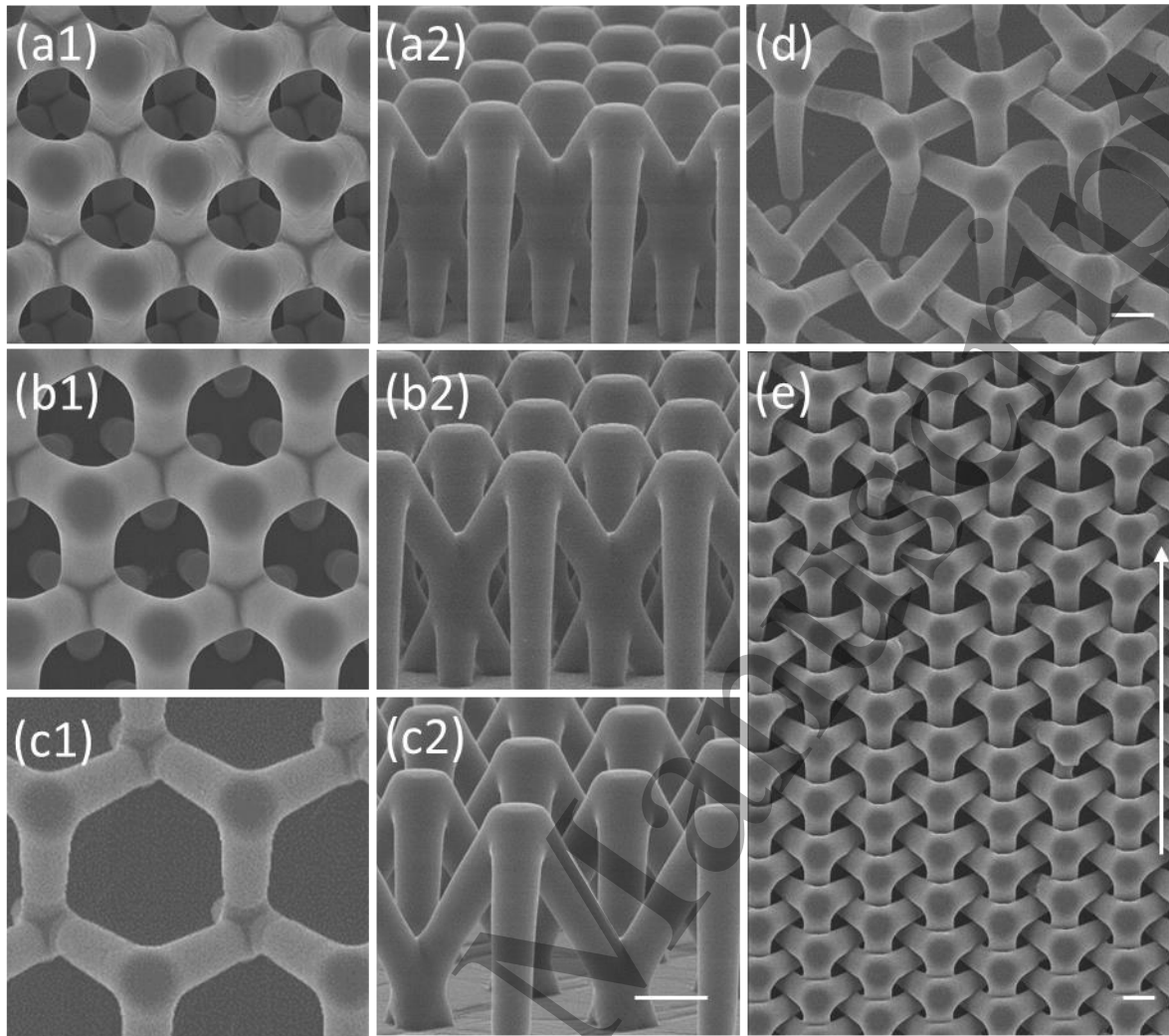
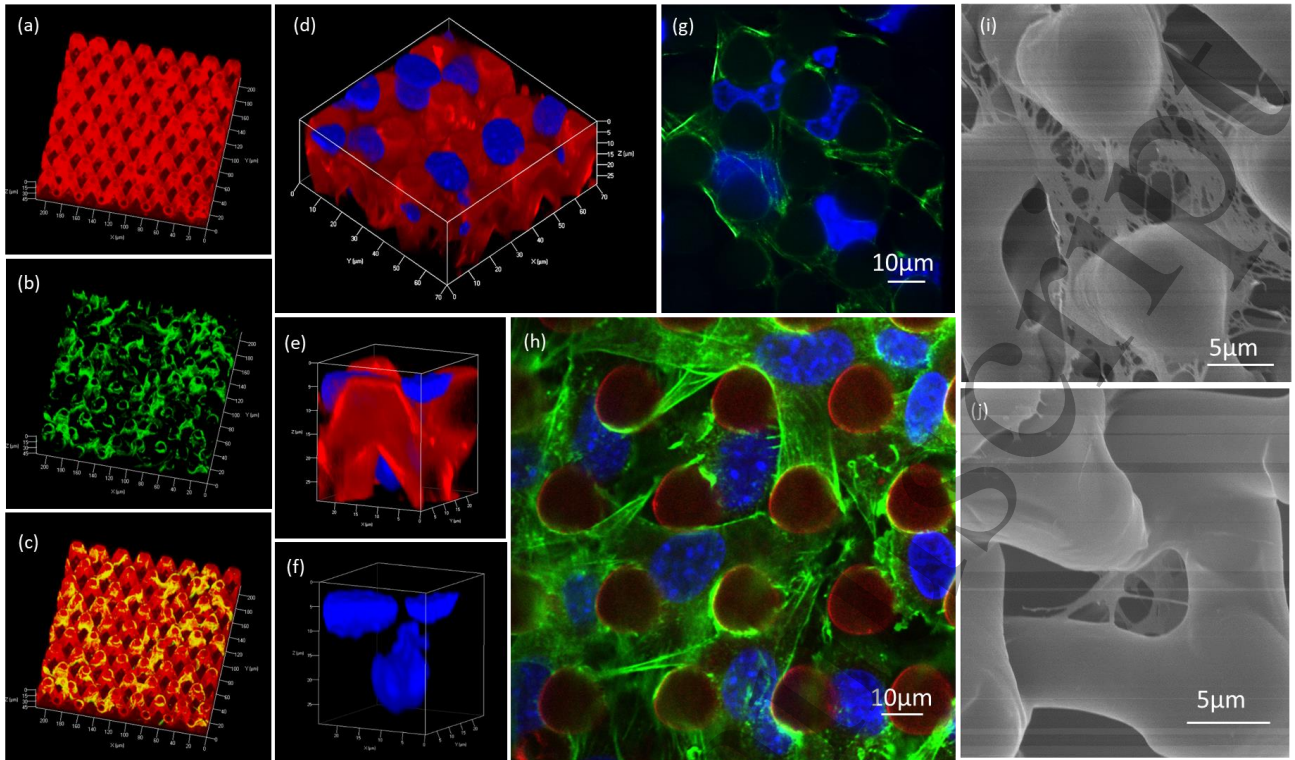
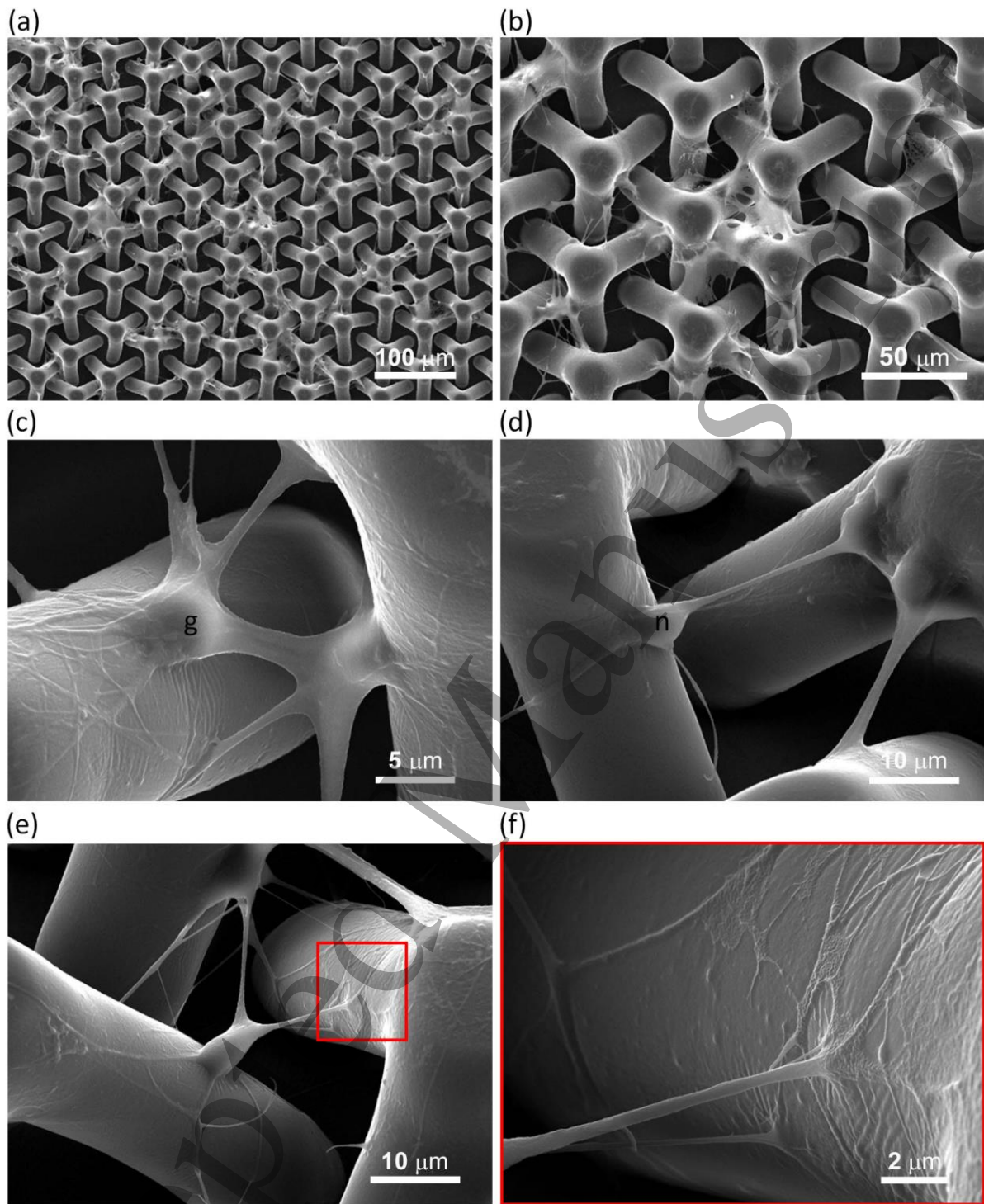


Figure 6



450 Figure 7



454 Figure 8

